An Automatic Denoising Method for NMR Spectroscopy Based on Low-Rank Hankel Model

Tianyu Qiu[®], Wenjing Liao[®], Yihui Huang[®], Jinyu Wu[®], Di Guo[®], Dongbao Liu[®], Xin Wang[®], Jian-Feng Cai[®], Bingwen Hu[®], and Xiaobo Qu[®], *Member, IEEE*

Abstract—Nuclear magnetic resonance (NMR) spectroscopy, whose time domain data is modeled as the sum of damped exponential signals, has become an indispensable tool in various scenarios, such as biomedicine, biology, and chemistry. NMR spectroscopy signals, however, are usually corrupted by Gaussian noise in practice, raising difficulties in sequential analysis and quantification. The low-rank Hankel property of exponential signals plays an important role in the denoising issue, but selecting an appropriate parameter still remains a problem. In this work, we explore the effect of the regularization parameter of a convex optimization denoising method based on low-rank Hankel matrices for exponential signals corrupted by Gaussian noise. An accurate estimate on the spectral norm of weighted Hankel matrices is provided as a guidance to set the regularization parameter. The bound can be efficiently calculated since it only depends on the standard deviation of the noise and a constant. Aided by the bound, one can easily obtain an auto-setting regularization parameter to produce promising denoised results. Our results on synthetic and realistic NMR spectroscopy data demonstrate a superior denoising performance of the proposed approach over typical Cadzow and the state-ofthe-art QR decomposition methods, especially in the low signalto-noise ratio regime.

Index Terms—Automatic parameter, Hankel matrix, nuclear magnetic resonance (NMR) spectroscopy, signal reconstruction, spectral denoising.

Manuscript received May 11, 2021; revised August 3, 2021; accepted August 19, 2021. Date of publication September 1, 2021; date of current version September 15, 2021. This work was supported in part by the National Natural Science Foundation of China under Grant 6212200447, Grant 61971361, Grant 61871341, and Grant 61811530021; in part by the National Key Research and Development Program of China under Grant 2017YFC0108703; in part by the Science and Technology Program of Xiamen under Grant 3502Z20183053; in part by the Health-Education Joint Research Project of Fujian Province under Grant 2019-WJ-31; and in part by Xiamen University Nanqiang Outstanding Talents Program. The Associate Editor coordinating the review process for this article was Dr. Lihui Peng. (Corresponding author: Xiaobo Qu.)

Tianyu Qiu, Yihui Huang, Jinyu Wu, Dongbao Liu, Xin Wang, and Xiaobo Qu are with Fujian Provincial Key Laboratory of Plasma and Magnetic Resonance, Biomedical Intelligent Cloud Research and Development Center, Department of Electronic Science, Xiamen University, Xiamen 361005, China (e-mail: quxiaobo@xmu.edu.cn).

Wenjing Liao is with the School of Mathematics, Georgia Institute of Technology, Atlanta, GA 30332 USA.

Di Guo is with Fujian Provincial University Key Laboratory of Internet of Things Application Technology, School of Computer and Information Engineering, Xiamen University of Technology, Xiamen 361024, China.

Jian-Feng Cai is with the Department of Mathematics, The Hong Kong University of Science and Technology, Hong Kong, China.

Bingwen Hu is with the Department of Physics, East China Normal University, Shanghai 200062, China.

This article has supplementary downloadable material available at https://doi.org/10.1109/TIM.2021.3109743, provided by the authors.

Digital Object Identifier 10.1109/TIM.2021.3109743

I. Introduction

UCLEAR magnetic resonance (NMR) spectroscopy has grown into an essential tool for biomedical studies [1], such as the structure determination [2], metabolic analysis [3], and medical diagnosis [4]. However, NMR spectroscopy signals are often corrupted by noise during acquisition and/or transmission. The noise problem turns out to be severe in the low signal-to-noise ratio (SNR) regime [5], [6]. Therefore, there is a strong demand for denoising signals, particularly in the low SNR regime.

Gaussian noise is commonly encountered in NMR spectroscopy denoising applications [7]–[10]. One of the most effective and widely adopted approaches to suppress Gaussian noise is to average multiple signal acquisitions. However, the multiple acquisitions are not always available or too costly in real applications. For this reason, effective denoising of the signals with a limited number of scans is favorable.

Numerous efforts have been made to denoise NMR spectroscopy signals. Among them, exploiting the exponential characteristic of NMR spectroscopy signals has been grown into a powerful tool [11]–[18]. Such low-rank properties were also utilized in NMR spectroscopy reconstruction [9], [14], [19]–[21], NMR spectroscopic imaging [22]–[24], and magnetic resonance imaging [25]-[27]. The Cadzow enhancement approach is popular in spectra denoising with the exploitation of the low-rank property of exponentials [11]-[13]. Compared with some typical denoising methods, such as the smoothing approach [28], wavelet thresholding [29], [30], maximum entropy [31], and covariance matrix [32], [33], Cadzow method is more theoretically adopted to the denoising of all NMR spectroscopy signals. However, it is a challenging task to choose a proper number R of exponential components in practical applications, unless a priori information is given. Efforts have been made to estimate R, such as the indicator function [34] and the significance level function [35], but the estimation of R may not be satisfactory enough to yield good results [36]. Another denoising method called random QR denoising method (rQRd) is based on an approximate low-rank decomposition and accelerates the computation by avoiding the singular value decomposition (SVD) in the Cadzow method [7]. It is, however, also based on an estimation of the rank R.

This low-rank Hankel property can also be exploited in an unconstrained convex optimization method for the reconstruction issue [14], [37]. The method, known as Low-Rank

1557-9662 © 2021 IEEE. Personal use is permitted, but republication/redistribution requires IEEE permission. See https://www.ieee.org/publications/rights/index.html for more information.

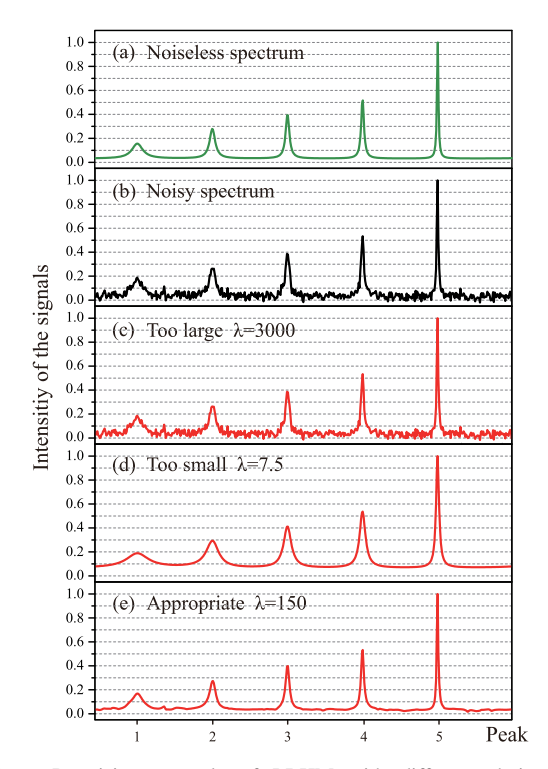


Fig. 1. Denoising example of LRHM with different choices of λ . (a) Noiseless spectrum. (b) Noisy spectrum with Gaussian noise ($\sigma=0.02$). (c)–(e) Denoised results with $\lambda=3000,\ 7.5,\$ and 150, respectively. Note: Without explicit illustration, λ is in the data consistency term in this article. The model of LRHM is written as $\min_{\mathbf{x}\in\mathbb{C}^{2N+1}}\|\mathcal{R}\mathbf{x}\|_* + (\lambda/2)\|\mathbf{y}-\mathbf{x}\|_2^2$.

Hankel Matrix reconstruction method (LRHM), can also be used for denoising, and one may receive a good result. The regularization parameter λ plays an important role in the results. As an example, Fig. 1 shows the denoised results with different λ . If λ is too large, the majority of the noise remains since the effect of the nuclear norm minimization is ignorable; if λ is too small, the spectral peaks are seriously distorted. Unfortunately, the choice of λ is still based on users' experience. Exploring the effect and the proper choice of λ is still of great demand and challenging.

In this article, we explore the effect of the regularization parameter and show that a good λ can be automatically chosen according to the spectral norm of a weighted Hankel matrix, which is estimated by random matrix theory as a guideline for the selection of a proper λ . One only needs to estimate the standard deviation of the noise, which can also be set automatically, to calculate this proper λ . Numerical experiments on both synthetic and real NMR spectroscopy data show that noise can be effectively removed when the parameter is chosen according to our analysis.

The rest of the article is organized as follows. Section II briefly reviews the signal model of NMR spectroscopy signals and LRHM in the denoising issue. Section III is devoted to analyzing the selection of λ and estimating the spectral norm of weighted Hankel matrices. Section IV contains numerical results on synthetic and real NMR spectroscopy data. Section V discusses the robustness to the estimate on the noise standard deviation, the effect of phase, the comparison with other methods, and the denoising on 13 C solid-state NMR

spectroscopy. Finally, we conclude and discuss future works in Section VI.

Notations used in the article are introduced below. We denote vectors through bold lowercase letters and matrices through bold uppercase letters. The entry in vectors and matrices is denoted by a normal letter with a subscript which stands for its location. For example, x_n denotes the nth element of \mathbf{x} , and $X_{m,n}$ denotes the (m,n)th entry of \mathbf{X} . For any vector \mathbf{x} , $\|\mathbf{x}\|_2$ represents the l_2 norm. For any matrix \mathbf{X} , $\|\mathbf{X}\|_*$ and $\|\mathbf{X}\|_2$ denote the nuclear norm and the spectral norm, respectively. The Hadamard product is denoted by \circ . We use superscript T and T to denote the transpose and the conjugate transpose of T and T to denote the transpose and the operators are denoted by calligraphic letters.

II. CONNECTION TO PRIOR WORK

In the time domain, NMR spectroscopy signal, referred to as free induction decay (FID), can be expressed as the sum of R exponentials

$$x_0(t_n) = \sum_{r=1}^R a_r e^{(j2\pi f_r - \tau_r)t_n}, \quad n = 0, \dots, 2N$$
 (1)

where a_r denotes the signal amplitude, f_r is the central frequency, and τ_r is the decay factor. When the number of peaks is small enough, usually $R \leq 0.1(N+1)$, the Hankel matrix can be treated as "low-rank" [14], [18]. In this work, we focus on the denoising of NMR spectroscopy with this property.

In practice, observations are often contaminated by noise and one receives $\mathbf{y} = \mathbf{x}_0 + \mathbf{z}$, where $\mathbf{x}_0 = \begin{bmatrix} x_0(t_0) \ x_0(t_1) \ , \dots, x_0(t_{2N}) \end{bmatrix}^T$ is a noiseless signal and $\mathbf{z} \in \mathbb{C}^{2N+1}$ is a random vector whose real and imaginary parts are independent identically distributed (i.i.d.) Gaussian with mean 0 and variance σ^2 .

Exponential signals can be transformed into Hankel matrices with a Vandermonde decomposition. Given \mathbf{x}_0 , one forms the square Hankel matrix

$$\mathcal{R}\mathbf{x}_{0} = \begin{bmatrix} x_{0}(t_{0}) & x_{0}(t_{1}) & \cdots & x_{0}(t_{N}) \\ x_{0}(t_{1}) & x_{0}(t_{2}) & \cdots & x_{0}(t_{N+1}) \\ \vdots & \vdots & \vdots & \vdots \\ x_{0}(t_{N}) & x_{0}(t_{N+1}) & \cdots & x_{0}(t_{2N}) \end{bmatrix}$$

where $\mathcal{R}: \mathbb{C}^{2N+1} \to \mathbb{C}^{(N+1)\times (N+1)}$ is the operator transforming a vector to the square Hankel matrix. It is well known that Rank $(\mathcal{R}\mathbf{x}_0) \leq R$ [38], [39].

The denoising method we explore is based on the low-rank property of $\mathcal{R}\mathbf{x}_0$ [14], and called Convex Hankel lOw-Rank matrix approximation for Denoising exponential signals. (CHORD), where one solves the following optimization problem:

$$\hat{\mathbf{x}} = \arg\min_{\mathbf{x} \in \mathbb{C}^{2N+1}} \|\mathcal{R}\mathbf{x}\|_* + \frac{\lambda}{2} \|\mathbf{y} - \mathbf{x}\|_2^2$$
 (2)

where λ denotes the regularization parameter and $\hat{\mathbf{x}}$ denotes the minimizer. The nuclear norm $\|\cdot\|_*$ is a surrogate for the rank [40].

Alternating direction method of multipliers (ADMM) [41] is a typical iterative algorithm, which can be used to solve (2). All details have been presented in the supplementary material (Section I).

The optimization problem in (2) involves a single regularization parameter λ and the denoised result crucially depends on the choice of λ . Therefore, setting an appropriate λ is a crucial issue in this denoising method. This article provides an automatic estimate on the proper choice of λ and validations by experimental results.

III. AUTOMATIC ESTIMATE OF THE REGULARIZATION PARAMETER λ

This section provides an estimate of the proper λ through establishing a relation between λ and the spectral norm of weighted Hankel matrices.

As $\hat{\mathbf{x}}$ is the minimizer of (2), according to the subgradient of the nuclear norm [40], [42]–[44], the subgradient of (2) is derived as

$$\lambda(\mathbf{y} - \hat{\mathbf{x}}) = \mathcal{R}^* \Big(\hat{\mathbf{U}} \hat{\mathbf{V}}^H + \hat{\mathbf{W}} \Big)$$
 (3)

where matrices $\hat{\mathbf{U}}$ and $\hat{\mathbf{V}} \in \mathbb{C}^{(N+1)\times(N+1)}$ are from the SVD of $\mathcal{R}\hat{\mathbf{x}}$ such that $\mathcal{R}\hat{\mathbf{x}} = \hat{\mathbf{U}}\hat{\mathbf{\Sigma}}\hat{\mathbf{V}}^H$ and $\hat{\mathbf{W}} \in \mathbb{C}^{(N+1)\times(N+1)}$ satisfy $\hat{\mathbf{U}}^H\hat{\mathbf{W}} = \mathbf{0}$, $\hat{\mathbf{W}}\hat{\mathbf{V}} = \mathbf{0}$, and $\|\hat{\mathbf{W}}\|_2 \leq 1$. $\hat{\mathbf{x}}$ should satisfy (3) for a matrix $\hat{\mathbf{W}}$ that has the aforementioned properties. \mathcal{R}^* : $\mathbb{C}^{(N+1)\times(N+1)} \to \mathbb{C}^{2N+1}$ is an operator transforming a matrix into vector via summing each antidiagonal.

Denote the vector \mathbf{w} is the weights defined as $\mathbf{w} = \begin{bmatrix} 1 \ 2 \ \dots, \ N+1 \ \dots, \ 2 \ 1 \end{bmatrix}^{\mathrm{T}} \in \mathbb{R}^{2N+1}$ and the symbol \circ stands for Hadamard product.

Since λ comes from the subgradient of (2), the optimal λ definitely satisfies (3). To obtain a specific λ value, it is necessary to know $\hat{\mathbf{U}}$, $\hat{\mathbf{V}}$, and $\hat{\mathbf{W}}$. However, according to the definition of the subgradient of the nuclear norm, the matrix $\hat{\mathbf{W}}$ cannot be obtained directly, so we have to use the inequality scaling and numerical experiments to obtain a proper λ .

Because $\lambda \mathcal{R}(1/\mathbf{w}) \circ (\mathbf{x}_0 + \mathbf{z} - \hat{\mathbf{x}})$ is an approximation of $\hat{\mathbf{U}}\hat{\mathbf{V}}^H + \hat{\mathbf{W}}$ and $\|\lambda \mathcal{R}(1/\mathbf{w}) \circ (\mathbf{x}_0 + \mathbf{z} - \hat{\mathbf{x}})\|_F \leq \|\hat{\mathbf{U}}\hat{\mathbf{V}}^H + \hat{\mathbf{W}}\|_F$ [11]. This relationship approximately holds in the spectral norm (see the details in the Supplement Section II). Therefore, the proper λ is chosen as

$$\lambda \leq \frac{1}{\|\mathbf{Z} + \tilde{\mathbf{X}}\|_{2}} \leq \frac{1}{\left(\left|\|\mathbf{Z}\|_{2} - \|\tilde{\mathbf{X}}\|_{2}\right|\right)}$$
(4)

where $\mathbf{Z} = (\mathcal{R}(1/\mathbf{w})) \circ \mathcal{R}\mathbf{z}$ denotes a weighted Hankel matrix such that

$$\mathbf{Z} = \left(\mathcal{R}\frac{1}{\mathbf{w}}\right) \circ \mathcal{R}\mathbf{z} = \begin{pmatrix} z_1 & \frac{z_2}{2} & \cdots & \frac{z_{N+1}}{N+1} \\ \frac{z_2}{2} & \frac{z_3}{3} & \cdots & \frac{z_{N+2}}{N} \\ \vdots & \vdots & \cdots & \vdots \\ \frac{z_{N+1}}{N+1} & \frac{z_{N+2}}{N} & \cdots & z_{2N+1} \end{pmatrix}$$
(5)

and $\tilde{\mathbf{X}}$ denotes $\tilde{\mathbf{X}} = (\mathcal{R}(1/\mathbf{w})) \circ \mathcal{R}(\mathbf{x}_0 - \hat{\mathbf{x}})$.

In order to explore the relationship among the spectral norm of weighted Hankel matrices, the noise level, and the size of

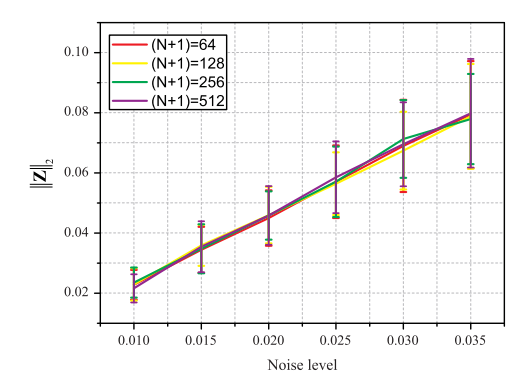


Fig. 2. Relation between $\|\mathbf{Z}\|_2$ and the standard deviation σ of the Gaussian noise \mathbf{z} in 100 Monte Carlo trials. The matrix \mathbf{Z} is of size $(N+1)\times(N+1)$ with (N+1)=64, 128, 256, and 512, respectively. The curve represents the mean of $\|\mathbf{Z}\|_2$ in 100 trials versus σ , and the standard deviation of $\|\mathbf{Z}\|_2$ in 100 trials is indicated by the vertical bar.

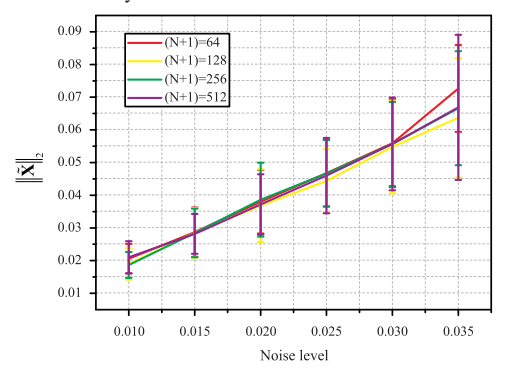


Fig. 3. Relation between $\|\tilde{\mathbf{X}}\|_2$ and the standard deviation σ of the Gaussian noise \mathbf{z} in 50 Monte Carlo trials. The matrix $\tilde{\mathbf{X}}$ is of size $(N+1)\times(N+1)$ with (N+1)=64, 128, 256, and 512, respectively. The curve represents the mean of $\|\tilde{\mathbf{X}}\|_2$ in 50 trials versus σ , and the standard deviation of $\|\tilde{\mathbf{X}}\|_2$ in 50 trials indicated by the vertical bar. Note: \mathbf{x}_0 are damped exponential signals with random a_r , f_r , and τ_r . $\hat{\mathbf{x}}$ is obtained from CHORD. The parameter λ is chosen such that the NRMSE is minimized.

the matrix, we did sufficient Monte Carlo trials on synthetic data and Gaussian noise. Results in Figs. 2 and 3 show that the empirical means of $\|\mathbf{Z}\|_2$ and $\|\tilde{\mathbf{X}}\|_2$ are almost independent of N. Furthermore, these empirical means increase as the increasing of the standard deviation σ of the noise.

In applications, it is expected that signal details can be preserved as much as possible, thus we propose to select the regularization parameter as

$$\lambda^* = \frac{1}{\left| \mathbb{E} \|\mathbf{Z}\|_2 - \mathbb{E} \|\tilde{\mathbf{X}}\|_2 \right|} \tag{6}$$

where the symbol \mathbb{E} denotes the expectation.

In order to provide a proper choice of λ , we estimate an upper and lower bound of $\mathbb{E}\|\mathbf{Z}\|_2$. With respect to $\mathbb{E}\|\tilde{\mathbf{X}}\|_2$, we provide an empirical value based on sufficient numerical experiments on synthetic data.

A. Bounds of $\mathbb{E}\|\mathbf{Z}\|_2$

Actually, for estimating bounds of the spectral norm of Hankel matrices given by random vectors, numerical achievements have been made [45]–[48]. In this section, we focus on estimating bounds of the spectral norm of weighted Hankel matrices. Theorems 1 and 2 provide a lower and upper bounds of $\mathbb{E}\|\mathbf{Z}\|_2$, respectively. All details of proofs and the asymptotic

analysis have been presented in the supplementary material (Sections III–V).

Theorem 1: Suppose the real and imaginary parts of the entries in $\mathbf{z} \in \mathbb{C}^{2N+1}$ are i.i.d. Gaussian random variables with mean 0 and variance σ^2 . Define R_N and Q_N such that

$$R_N^2 = \sum_{k=0}^{2N} |d_k|^2$$
 and $Q_N^4 = \sum_{k=0}^{2N} |d_k|^4$ (7)

where

$$d_k = \begin{cases} \frac{2}{(k+1)(k+2)} \sum_{m=0}^k \frac{1}{m+1}, & 0 \le k \le N\\ \frac{2}{(2N-k+1)(k+2)} \sum_{m=k}^{2N} \frac{1}{m-N+1}, & N < k \le 2N. \end{cases}$$

Then there exists a constant C such that the matrix \mathbf{Z} defined in (4) satisfies

$$\mathbb{E}\|\mathbf{Z}\|_{2} \ge \sigma \frac{C(N+1)}{2N+1} \sqrt{R_{N}^{2} \left(1 + \log \frac{R_{N}^{4}}{Q_{N}^{4}}\right)}.$$
 (8)

Theorem 2: Suppose the real and imaginary parts of the entries in $\mathbf{z} \in \mathbb{C}^{2N+1}$ are i.i.d. Gaussian random variables with mean 0 and variance σ^2 . Then

$$\mathbb{E}\|\mathbf{Z}\|_{2} \le \sigma \sqrt{2C_{\mathbf{w}}\log(2N+2)} \tag{9}$$

where $C_{\mathbf{w}} = \max(\sum_{k=0}^{N} w_k^{-2}, \sum_{k=1}^{N+1} w_k^{-2}, \dots, \sum_{k=N}^{2N} w_k^{-2})$ with the vector \mathbf{w} defined in (5).

The above two theorems provide the following upper and lower bounds of $\mathbb{E}\|\mathbf{Z}\|_2$:

$$\sigma \frac{C(N+1)}{2N+1} \sqrt{R_N^2 \left(1 + \log \frac{R_N^4}{Q_N^4}\right)}$$

$$\leq \mathbb{E} \|\mathbf{Z}\|_2 \leq \sigma \sqrt{2C_{\mathbf{w}} \log(2N+2)}. \quad (10)$$

The upper bound scales as $\sigma(\log N)^{1/2}$, while the lower bound depends on R_N and Q_N . When N is large enough, the upper bound and the lower bound only differ by a factor of $(\log N)^{1/2}$.

Choosing the lower bound of $\mathbb{E}\|\mathbf{Z}\|_2$ tends to obtain a relatively large λ , which is beneficial to preserve more signal details. Therefore, we suggest to choose $\mathbb{E}\|\mathbf{Z}\|_2$ as

$$\mathbb{E}\|\mathbf{Z}\|_{2} = \frac{C(N+1)}{(2N+1)} \sqrt{R_{N}^{2} \left(1 + \log \frac{R_{N}^{4}}{Q_{N}^{4}}\right)} \sigma. \tag{11}$$

We next find the empirical constant C through repetitive experiments on synthetic data. According to Theorem 1, C>0 is a constant, which is independent of the signal length and the standard deviation σ .

The slope values of lines in Fig. 2 are estimated by the least-square method. According to the conclusion in (9), C values are obtained via dividing slopes by $(N+1)/(2N+1)(R_N^2(1+\log(R_N^4/Q_N^4)))^{1/2}$. Finally, after averaging four C values, we suggest that C=2.9 for denoising. Results in Fig. 4 confirm that the conclusion in Theorem 1 is well capable of estimating $\mathbb{E}\|\mathbf{Z}\|_2$.

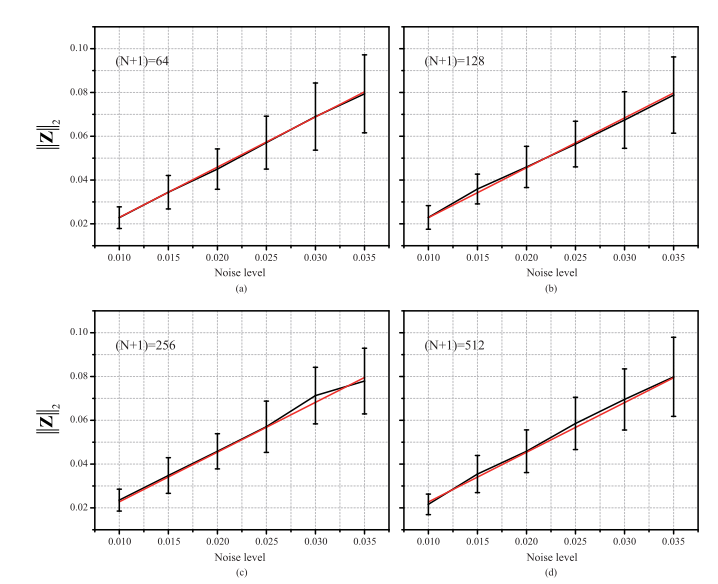


Fig. 4. $\mathbb{E}\|\mathbf{Z}\|_2$ and the lower bound with the suggested C under different matrix sizes. The matrix \mathbf{Z} is of size $(N+1)\times(N+1)$ with (N+1)=64 (a), 128 (b), 256 (c), and 512 (d), respectively. The vertical axis denotes the value of $\|\mathbf{Z}\|_2$ and the horizontal axis denotes the standard deviation of Gaussian noise. The black curves stand for the empirical mean of $\|\mathbf{Z}\|_2$ in Fig. 2. Red lines denote the lower bounds with C=2.9. The error bars denote the standard deviation of $\|\mathbf{Z}\|_2$ values in 100 Monte Carlo trials.

B. Empirical $\mathbb{E}\|\mathbf{\tilde{X}}\|_{2}$

This section is devoted to an empirical estimate of $\mathbb{E} \| \tilde{\mathbf{X}} \|_2$. We perform experiments with different N, σ , λ , signals, and noises in order to determine a proper empirical estimate value.

Before evaluating the denoising performance, we first introduce two objective criteria, normalized root-mean-square error (NRMSE) [49] and mean absolute error (MAE) [50]

$$NRMSE = \frac{\|\hat{\mathbf{x}} - \mathbf{x}_0\|_2}{\|\mathbf{x}_0\|_2}$$
 (12)

where $\hat{\mathbf{x}}$ and \mathbf{x}_0 are the denoised signal and the noiseless signal, respectively.

$$MAE = \frac{\|\mathbf{f}_s - \mathbf{f}_0\|_1}{2N + 1}$$
 (13)

where $\mathbf{f}_s \in \mathbb{R}^{(2N+1)\times 1}$ and $\mathbf{f}_0 \in \mathbb{R}^{(2N+1)\times 1}$ denote the real part of the noisy spectrum and the noiseless spectrum, respectively.

We generate a synthetic dataset, including 90 random damping complex exponential signals with 2N + 1 = 255, 511, and 1023, respectively, and repeat 100 Monte Carlo trials to incorporate the randomness of Gaussian noise. Each signal in the dataset has 3R + 1 parameters, including R, a_r , f_r , and τ_r , where r = 1, 2, ..., R. The number of exponential components is $R = 4+M_r$, where M_r denotes a pseudorandom scalar integer of range [1, 9]. The amplitude a_r is uniformly sampled from (0, 10). Each frequency f_r is uniformly sampled from (0, 1). The damping factor is $\tau_r = 5 + 60m_r$, where m_r is uniformly sampled from (0, 1).

Then, we use a series of λ to denoise signals in the dataset above, find the optimal solution $\hat{\mathbf{x}}$ corresponded to the lowest error, NRMSE, and calculate $\|\tilde{\mathbf{X}}\|_2$. Nine signals with different data lengths are randomly selected and the corresponding $\|\tilde{\mathbf{X}}\|_2$ are presented in Fig. 5.

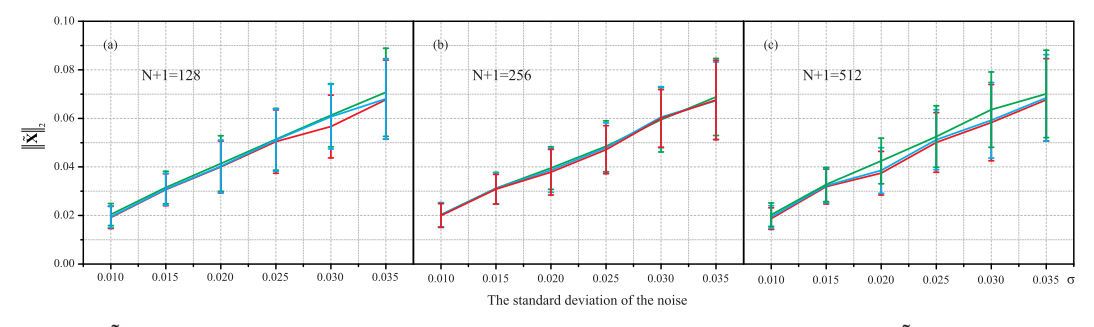


Fig. 5. Relation between $\|\tilde{\mathbf{X}}\|_2$ given by random synthetic signals and noise levels. (a)–(c) Average spectral norm of $\tilde{\mathbf{X}}$ which is of size $(N+1)\times(N+1)$ with (N+1)=128 (a), 256 (b), 512 (c), respectively. The vertical error bars represent the standard deviation of $\|\tilde{\mathbf{X}}\|_2$ values in 100 Monte Carlo trials. Note: For each subplot, the green, blue, and red lines denote $\|\tilde{\mathbf{X}}\|_2$ given by different random signals.

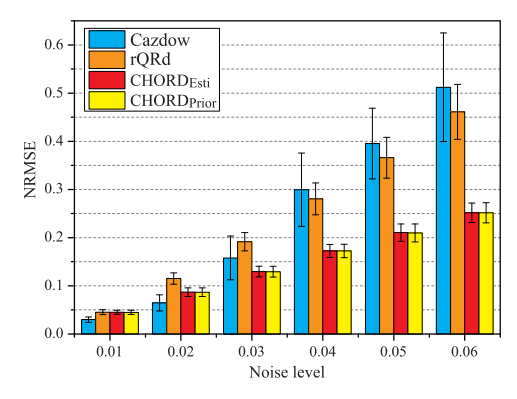


Fig. 6. Reconstruction error, NRMSE, for synthetic data [Fig. 1(a)] under different noise levels. CHORD_{Esti} and CHORD_{Prior} denote denoised results of CHORD with estimated standard deviation and the known standard deviation, respectively. Cadzow and rQRd present the optimal (minimal NRMSE) denoised results, respectively. The height of columns shows the average of the NRMSEs over 100 trials. The vertical bar comes from the randomness of noise.

Results in Fig. 5 indicate that the standard deviation of noise is the main factor that determines $\mathbb{E}\|\tilde{\mathbf{X}}\|_2$. Moreover, this empirical mean of $\|\tilde{\mathbf{X}}\|_2$ seems to be linear to the standard deviation of the noise. Additionally, the spectral parameters and the distribution they satisfy also slightly affects $\mathbb{E}\|\tilde{\mathbf{X}}\|_2$ (see the details in the supplementary material Section IX). We estimate the slope on MATLAB platform (2017b) and suggest $\mathbb{E}\|\tilde{\mathbf{X}}\|_2 = 1.94\sigma$ for denoising.

IV. NUMERICAL EXPERIMENTS

In this section, we evaluate the performance of CHORD with the suggested λ on the synthetic data and a realistic NMR spectroscopy dataset. No preprocessing, including the phase correction and apodization, was applied to the synthetic data. For the data acquired from real NMR spectrometer, we merely truncated the FID signal and only used the first 1000 points. For visualization, real-part spectra are presented and imaginary-part spectra are discarded, but all the processing are on complex data. In addition, for avoiding the bias, the proposed method has also been tested on random simulated data, whose detailed results are presented in the supplementary material (Section X).

The typical method, Cadzow [7], [13], and the state-of-the-art method, rQRd [7], are compared with our proposed method. For Cadzow, its key parameter is the rank of this Hankel matrix. For rQRd, its primary parameter is the number of the matrix \mathbf{Q} 's column, denoted as rank $_{Q}$, in QR

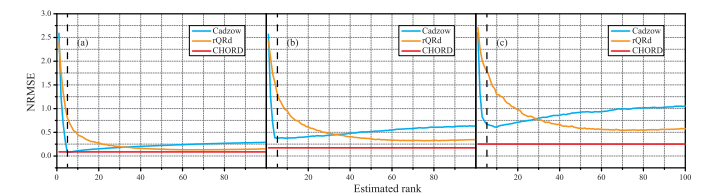


Fig. 7. Average NRMSE of denoised results of the synthetic data [in Fig. 1(a)] with different estimated ranks over 50 Mont Carlo trials. (a)–(c) Average NRMSE of denoised results with $\sigma=0.02,\,0.04,\,$ and 0.06, respectively. The black dash lines stand for the exact rank of the synthetic data (rank = 5). Note: For rQRd, the estimated rank stands for rank $_Q$.

decomposition. For the rest of the manuscript, without explicit illustration, the main parameters in Cadzow and rQRd are chosen to be the ones yielding the lowest reconstruction error, NRMSE.

A. Denoising of Synthetic Complex Data

We generated a synthetic exponential complex data with five peaks [presented in Fig. 1(a)]. In the following, the synthetic data indicates the signal in Fig. 1(a). The denoising performance of the three methods is tested through recovering the signal from complex Gaussian noise with different standard deviation ($\sigma = 0.01, 0.02, 0.03, 0.04, 0.05,$ and 0.06, respectively). 100 Monte Carlo trials are done to avoid the randomness of noise.

In practice, we do not know in advance the standard deviation of the noise that corrupts the signal of interest. Here, we truncate the signal from the end of noisy FID to estimate the standard deviation of the noise to mimic the real cases. The truncated length is verified by Kolmogorov–Smirnov (KS) test [51]. Also, we compare the denoising performance of CHORD given the known standard deviation and the estimated standard deviation. For clarity, we name the CHORD using the known standard deviation CHORD_{Prior} and the CHORD using estimated standard deviation CHORD_{Esti}, respectively.

Fig. 6 shows the denoising performance under different noise levels. Under relatively weak noise ($\sigma \leq 0.02$), Cadzow achieves the lowest NRMSE compared to other approaches. Under relatively high noise ($\sigma \geq 0.05$), however, the NRMSE of Cadzow increases faster than that of rQRd and, particularly, CHORD, implying Cadzow is not robust to relatively high noise levels. The proposed method produces the lowest NRMSE when the noise is higher than 0.03 and produces smallest variances. Furthermore, the results of CHORD_{Esti} are very close to that of CHORD_{Prior}, showing the feasibility

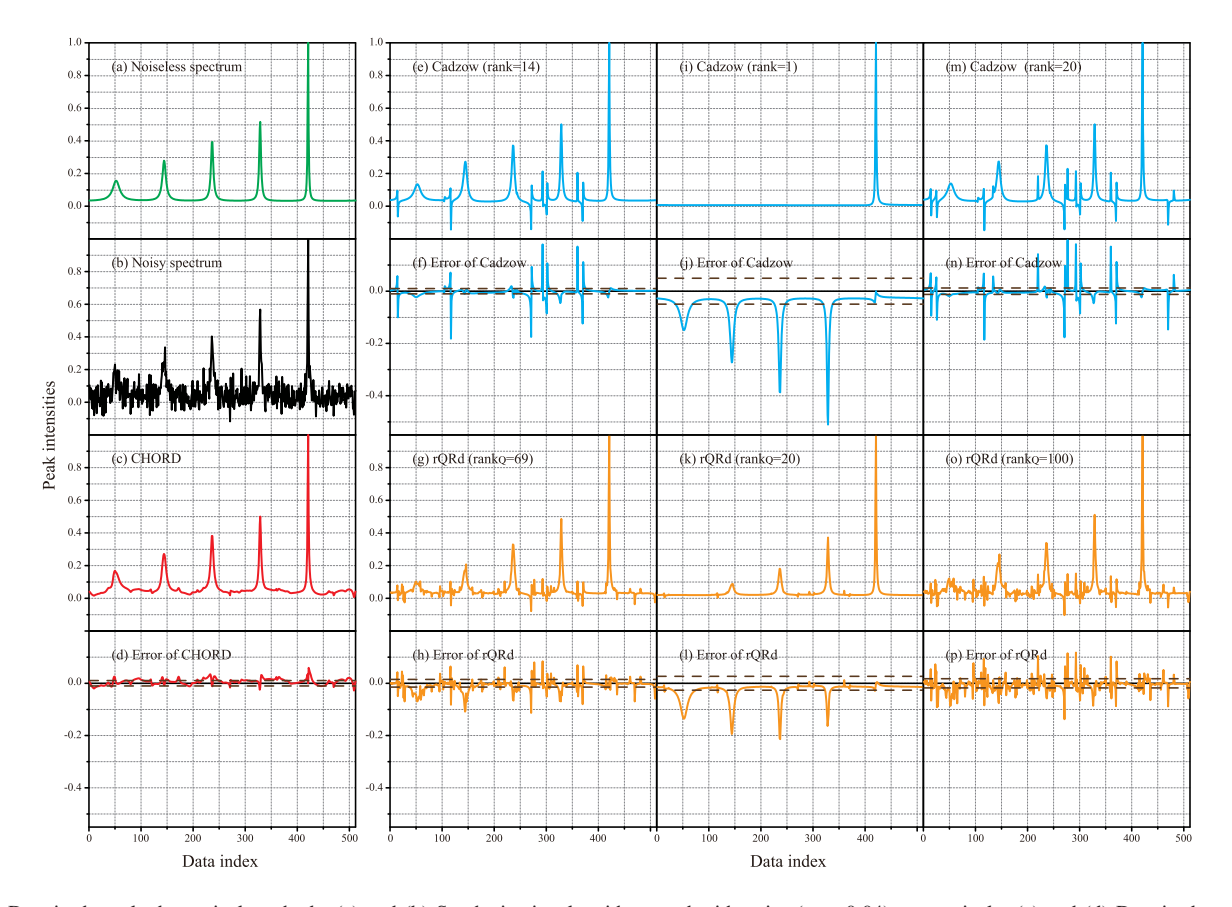


Fig. 8. Denoised results by typical methods. (a) and (b) Synthetic signals without and with noise ($\sigma = 0.04$), respectively. (c) and (d) Denoised spectra and errors of CHORD with the suggested parameter. (e) and (f), (i) and (j), and (m) and (n) Denoised spectra and errors of Cadzow with three different estimated ranks (optimal in terms of NRMSE, small, and large). (g) and (h), (k) and (l), and (o) and (p) Denoised results of rQRd with three different estimated ranks (optimal in terms of NRMSE, small, and large). The brown long dash lines denote the MAEs of the denoised spectra.

of CHORD. In the following, without explicit illustration, the mentioned CHORD is CHORD_{Esti}.

We evaluate the effect of parameter selection of the tested approaches in Fig. 7. For Cadzow, when the noise is weak [Fig. 7(a)], an accurate estimate leads to a good result. But as the noise gets stronger, the optimal estimated rank (in terms of NRMSE) may be not equivalent to the actual rank [Fig. 7(c)], meaning that if the noise level is strong enough, an accurate estimated rank will not significantly improve denoised results. Compared with Cadzow, rQRd owns a more flexible parameter setting, but the average NRMSE of its denoised results is always higher than that of CHORD under large noise.

Fig. 8 presents the representative denoised results of the synthetic signal corrupted by strong noise. Typical denoised spectra of Cadzow and rQRd with three different parameters selection are presented. Cadzow tends to remove small peaks if using a much smaller estimated rank [see Fig. 8(i)]. And if the estimated rank is close to or larger than the real rank, Cadzow spectra introduce spectral distortions and distinct artifacts [see Fig. 8(e) and (m)]. For rQRd, a small rank ϱ leads to a smooth spectrum but with missed or weakened low-intensity peaks [see Fig. 8(k)], while larger parameters introduce strong noise [see Fig. 8(g) and (o)]. For the CHORD, it provides a relatively reasonable denoised result using the suggested λ and the estimated noise level.

B. Denoising of NMR Spectroscopy Data

NMR spectroscopy, as a noninvasive technology, has been widely utilized in the study of chemistry, biology, and medicine, such as the diagnosis of diseases [22]. One of the reasons that limit the widespread of this technology is its relatively low SNR. Therefore, CHORD is evaluated on the denoising of a real NMR spectroscopy data. We acquired the signal with high SNR as the reference and added the Gaussian noise retrospectively.

In applications, the unit of chemical shift is usually expressed in part per million (ppm) instead of the hertz, avoiding the ambiguity when spectrometers are at different magnet strengths. The definition of chemical shift is given by

chemical shift(ppm) =
$$\frac{f_{\text{test}} - f_{\text{ref}}}{f_{\text{spec}}} \times 10^6$$
 (14)

where $f_{\rm test}$ denotes the resonance frequency of the sample, $f_{\rm ref}$ the absolute resonance frequency of a standard compound measured in the same magnetic field, and $f_{\rm spec}$ the frequency of the magnetic field strength of spectrometers.

The real data is a 1-D 1 H NMR spectrum that was acquired at 298 K on a Varian 500 MHz (11.7 T) magnetic resonance system (Agilent Technologies, Santa Clara, CA, USA) equipped with a 5-mm indirect detection probe. A 8.3 μ s

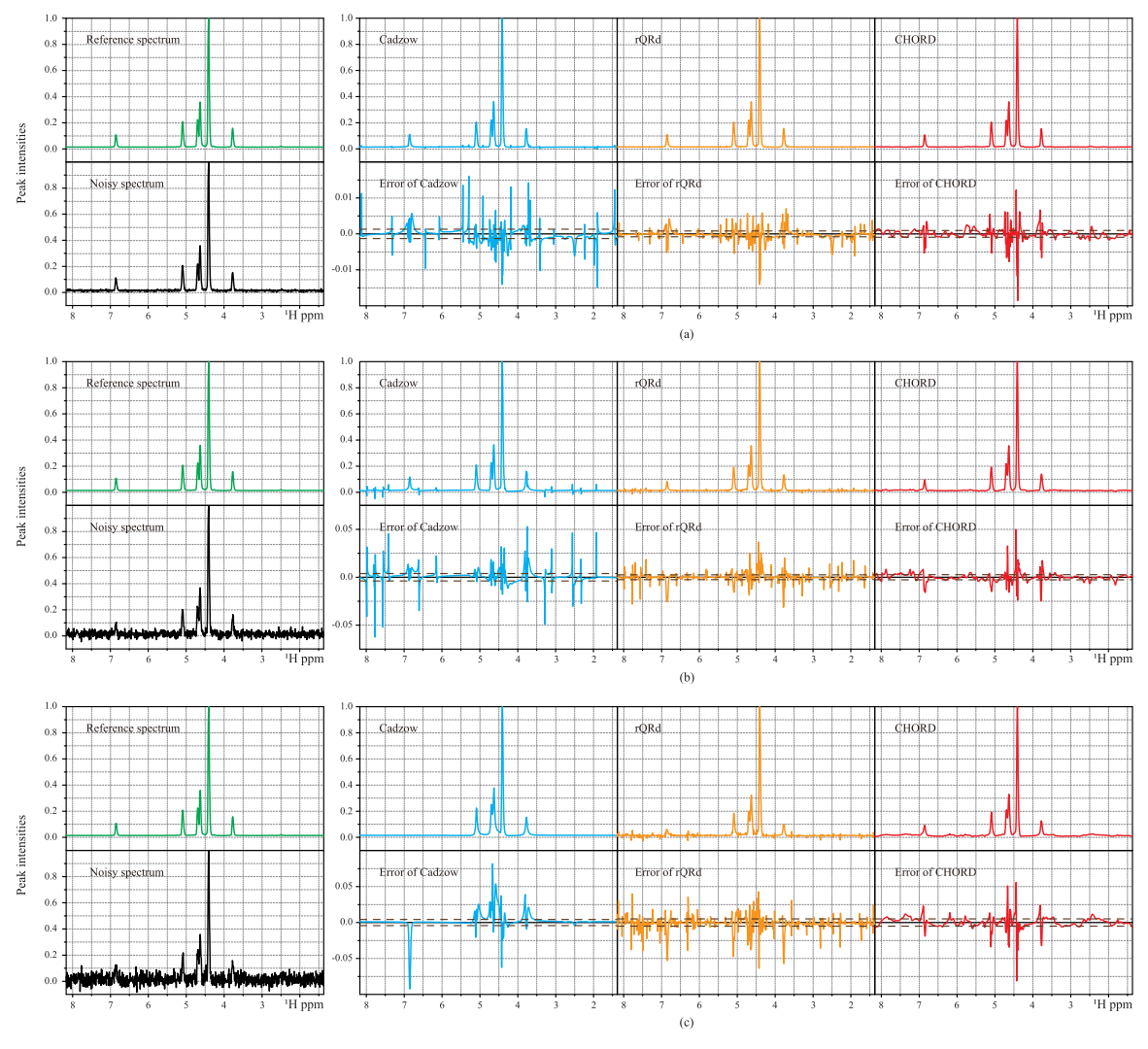


Fig. 9. Denoised results of realistic metabolite spectrum with $\sigma = 0.035$ (a), 0.020 (b), and 0.005 (c), respectively. The green lines denote the reference spectrum with high SNR. The black lines indicate noisy spectra. The blue, orange, and red lines are denoised results of Cadzow, rQRd, and CHORD, respectively. Note: The results of Cadzow and rQRd that enable the lowest NRMSE are presented here. The brown long dash lines denote the MAEs of the denoised spectra.

single-pulse sequence was used, and 64 scans were acquired. The total acquisition time took 286.7 s. The concentration of creatine, choline, magnesium citrate, and calcium citrate are 0.03, 0.03, 0.06, and 0.06 g/mL, respectively.

The denoised results of the metabolic spectrum are presented in Fig. 9, which supports the conclusion made on the synthetic data. Under a relatively strong noise level ($\sigma=0.035$), Cadzow smooths the spectrum, which, on the one side, offers a nice denoised results, on the other side, however, leads to the missing of some peaks (such as the peaks at 6.8 ppm). rQRd provides a spectrum with obvious noise [orange lines in Fig. 9(c)] and weakens low-intensity peaks (such as the peaks at 6.8 ppm). CHORD is capable of effectively removing noise and keeping more details of peaks [see Fig. 9(c)]. For the high SNR scenario, all the three methods produce nice and comparable denoised results [see Fig. 9(a)].

Experiments on synthetic complex exponential and realistic NMR spectroscopy data demonstrate that CHORD with the auto-setting parameter achieves more robust and accurate results compared with Cadzow and rQRd methods.

V. DISCUSSIONS

A. Estimate of Noise

We estimate the noise level by calculating the standard deviation of signals truncated from the end of noisy FIDs on MATLAB platform (2017b). To ensure that the truncated signals satisfy the Gaussian distribution, KS test is introduced into the noise estimate. Details of the *p*-value test and the flowchart have been shown in the Supplement (Section VI).

The *p*-values of different truncated lengths under various noise levels are tested on the simulated data (Fig. 10). 100 Monte Carlo trials have been done to avoid the randomness of noise.

The results in Fig. 10 illustrate that the reduction of p-values is caused by the truncation of FID. In the areas without noise, such as the last 200 points in Fig. 10(a), the average of p-values approximates 0.8. As the truncated length increases, a part of the signal is treated as noise, resulting in the apparent descent of p-values. Additionally, a low noise level is beneficial to distinguish the noise and the ground truth, which is reflected in the earlier decrease of p-values.

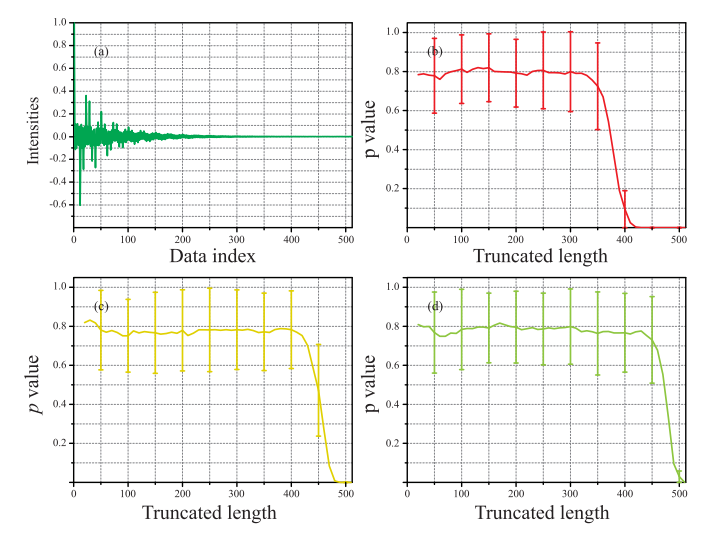


Fig. 10. p-values with different truncated lengths under various noise levels. (a) Synthetic FID signal in Fig. 8(a). (b)–(d) p-values of (a) under noise with $\sigma=0.01,\ 0.03,\$ and $0.05,\$ respectively.

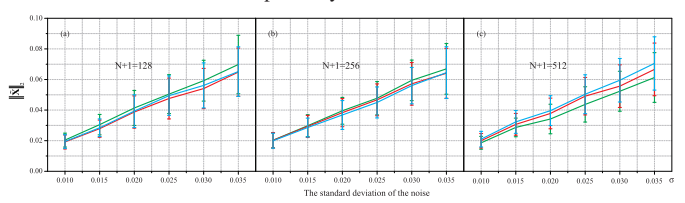


Fig. 11. Relation between $\|\tilde{\mathbf{X}}\|_2$ given by random synthetic signals with zero-order phases and noise levels. (a)–(c) Average spectral norm of $\tilde{\mathbf{X}}$ which is of size $(N+1)\times (N+1)$ with (N+1)=128,256, and 512, respectively. The vertical error bars come from 100 Monte Carlo trials. Note: For each subplot, the green, blue, and red lines denote $\|\tilde{\mathbf{X}}\|_2$ given by random signals with different spectral parameters.

Furthermore, *p*-values fluctuate at 0.8 for truncated signals without FID. Therefore, we selected 0.8 as the threshold value.

B. Effect of Phase on $\mathbb{E} \| \tilde{\mathbf{X}} \|_2$

Since the effect of phase can be alleviated by the correction in the preprocessing, in the above, we temporarily omitted the phase during the estimate of $\mathbb{E} \left\| \widetilde{\mathbf{X}} \right\|_2$ to simplify the problem. This section is devoted to discuss the empirical value of $\mathbb{E} \left\| \widetilde{\mathbf{X}} \right\|_2$ under two common situations where the signal x_0 contains the zero-order and relative phase.

Both the zero-order phase θ and the relative phase θ_r are uniformly random and sampled from (0, 1). These phases are added for the experiments as

(Zero-order phase)

$$x_0(t_n) = e^{j2\pi\theta} \sum_{r=1}^R a_r e^{(j2\pi f_r - \tau_r)t_n}, \quad n = 0, \dots, 2N \quad (15)$$

and

(Relative phase)

$$x_0(t_n) = \sum_{r=1}^R a_r e^{j2\pi\theta_r} e^{(j2\pi f_r - \tau_r)t_n}, \quad n = 0, \dots, 2N. \quad (16)$$

According to results of the Monte Carlo simulations (Figs. 11 and 12), it is observed that $\mathbb{E}\|\mathbf{\tilde{X}}\|_2$ tends to be

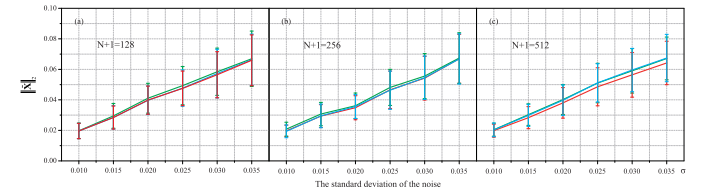


Fig. 12. Relation between $\|\tilde{\mathbf{X}}\|_2$ given by random synthetic signals with the relative phase. (a)–(c) Average spectral norm of $\tilde{\mathbf{X}}$ which is of size $(N+1) \times (N+1)$ with (N+1)=128,256, and 512, respectively. The vertical error bars come from 100 Monte Carlo trials. Note: For each subplot, the green, blue, and red lines denote $\|\tilde{\mathbf{X}}\|_2$ given by random signals with different spectral parameters.

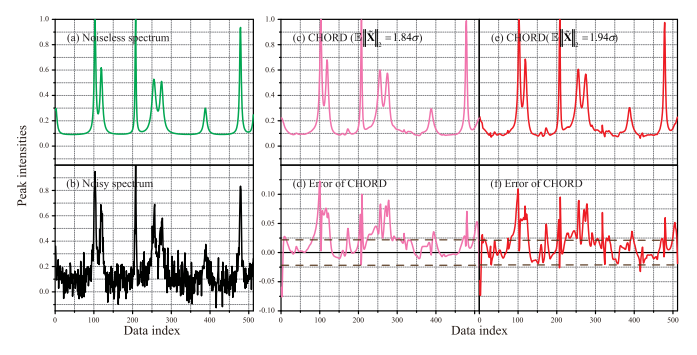


Fig. 13. Comparison of 512-point denoised spectra with the zero-order phase under the new and the suggested $\mathbb{E}\|\tilde{\mathbf{X}}\|_2$ values. (a) and (b) Synthetic signals without and with noise ($\sigma=0.02$). (c) and (e) Denoised spectra of CHORD with the new value (1.84 σ) and the suggested value (1.94 σ), respectively. (d) and (f) Denoising errors of spectra that correspond to (c) and (e), respectively. The brown long dash lines denote the MAEs of the denoised spectra.

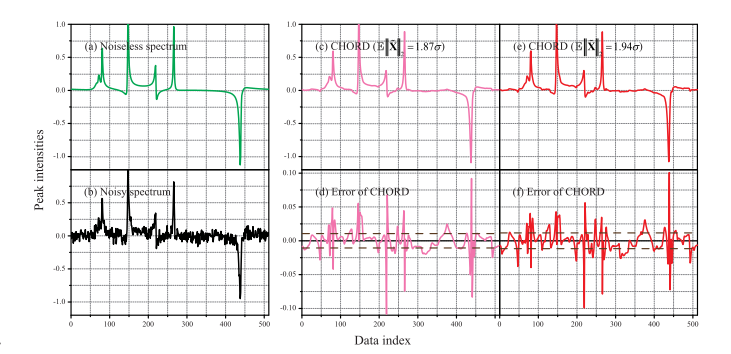


Fig. 14. Comparison of 512-point denoised spectra with the relative phase under the new and the suggested $\mathbb{E}\|\hat{\mathbf{X}}\|_2$ values. (a) and (b) Synthetic signals without and with noise ($\sigma=0.03$). (c) and (e) Denoised spectra of CHORD with the new value (1.87 σ) and the suggested value (1.94 σ), respectively. (d) and (f) Denoising errors of spectra that correspond to (c) and (e), respectively. The brown long dash lines denote the MAEs of the denoised spectra

proportional to the noise level. Utilizing the same technique in Section III-B, the empirical relation between $\mathbb{E}\|\tilde{\mathbf{X}}\|_2$ and the standard deviation of the noise can be acquired. Compared with the suggested value, the zero-order and relative phase slightly reduce $\mathbb{E}\|\tilde{\mathbf{X}}\|_2$. But this change causes little impact on the denoised spectra (Figs. 13 and 14).

The slopes of lines corresponding to all synthetic data with the zero-order phase were estimated by the least-square method, and the averaged slope is 1.84. Compared with the suggested value (1.94), the relative error is 5%. For synthetic

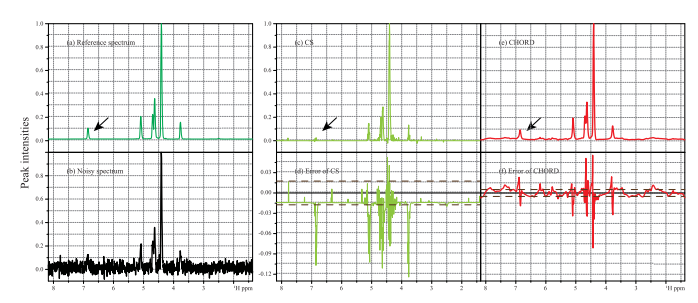


Fig. 15. Denoising of realistic metabolite spectrum by CS and CHORD. (a) Reference spectrum with high SNR. (b) Noisy spectrum ($\sigma=0.035$). (c) and (e) Denoised results by CS and CHORD, respectively. (d) and (f) Denoising error of two methods, respectively. The brown long dash lines denote the MAEs of the denoised spectra.

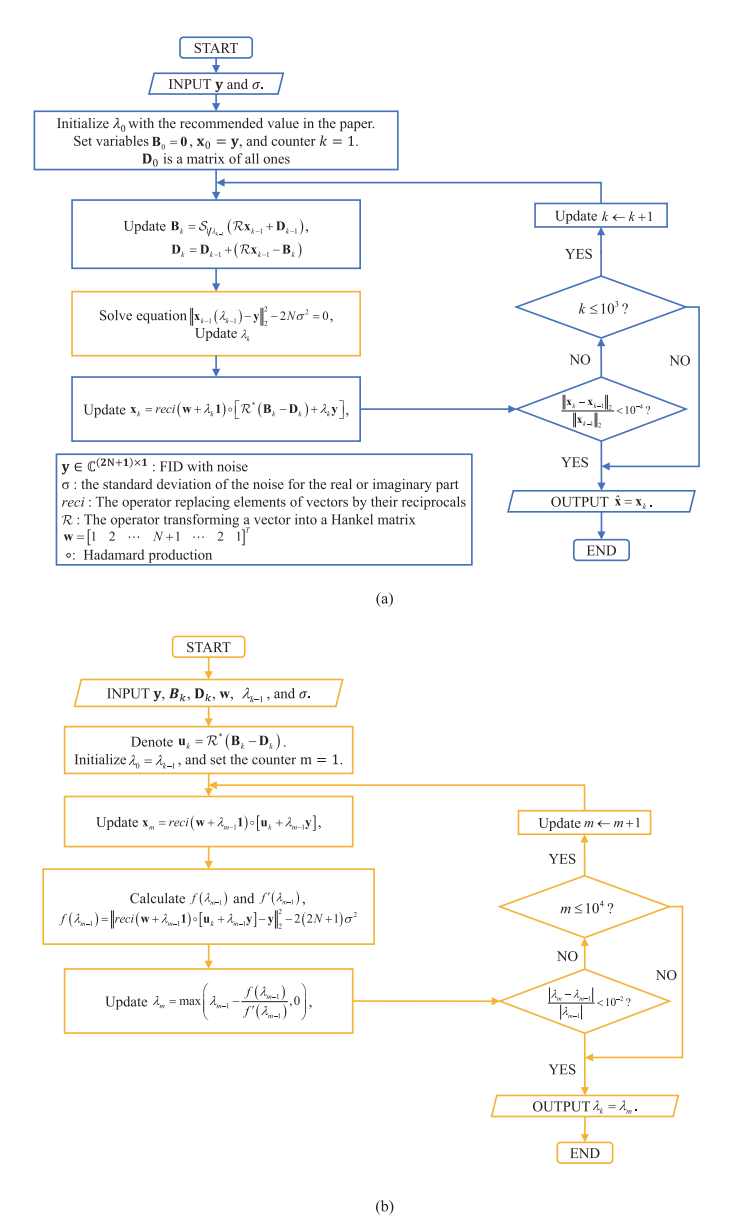


Fig. 16. Flowchart of CHORD-DP. (a) Flowchart of the whole algorithm. (b) Details of the orange box in (a).

data with the relative phase, the same technique is utilized to estimate the slope, and the average slope is 1.87. Compared with the suggested value, the relative error is 4%. In the

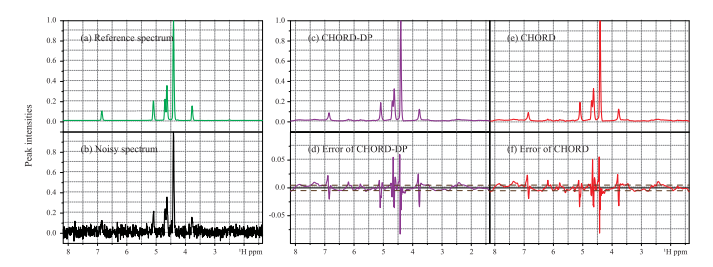


Fig. 17. Denoised results of the realistic metabolite spectrum. (a) Reference spectrum with high SNR. (b) Noisy spectrum ($\sigma=0.035$). (c) and (e) Denoised results by CHORD with parameter estimated by DP and the suggested parameter. (d) and (f) Denoising error of two methods. The brown long dash lines denote the MAEs of the denoised spectra.

supplementary material (Section VII), signals with 256 and 1024 data points are shown to complement the discussion.

C. Comparison with Other Representative Methods

This section, respectively, provides the comparison between the proposed method and two representative methods, a sparse regularization-based method, compressed sensing (CS) [52], and adaptive regularization parameters selection method with discrepancy principle (DP) [53]. We verify these methods on the denoising of the synthetic and the experimental NMR spectra. The synthetic denoised spectra and NRMSE are shown in the supplementary material (Section VIII).

- 1) Comparison with CS: The CS assumes the sparsity of NMR spectroscopy in the frequency domain. For the denoised spectra, CHORD better removes noise and retains peak details (such as the peak at 6.8 ppm in Fig. 15) than CS.
- 2) Comparison with DP-Based Method: The DP tries to find an optimal regularization parameter so that the norm of denoising error is equal to that of the noise [53]. DP has been used in Tikhonov regularization [53], total variation (TV) [54], and low-rank reconstruction [55].

We implemented a DP-based method (see Fig. 16) to select a λ^* to satisfy

$$\|\hat{\mathbf{x}}(\lambda^*) - \mathbf{y}\|_2 = C\sigma \tag{17}$$

where σ stands for the standard deviation of real/imaginary part of noise. C is a constant.

Spectra in Fig. 17 shows that both the proposed method and DP can remove the noise well, while the former obtains slightly lower NRMSE than the latter (see the supplementary material). However, the convergence of DP has not been proved in LRHM, which is worthy of further investigation in the future.

D. Denoising on ¹³C Solid-State NMR Spectroscopy

To evaluate the denoising performance under a more realistic scenario, we tested the performance of the proposed method (Fig. 18) on experimental ¹³C solid-state NMR spectra which were acquired with varying levels of average. Solid-state NMR spectroscopy has grown into a versatile tool to analyze materials in the solid state but is limited by a relatively low SNR due to its poor sensitivity [36].

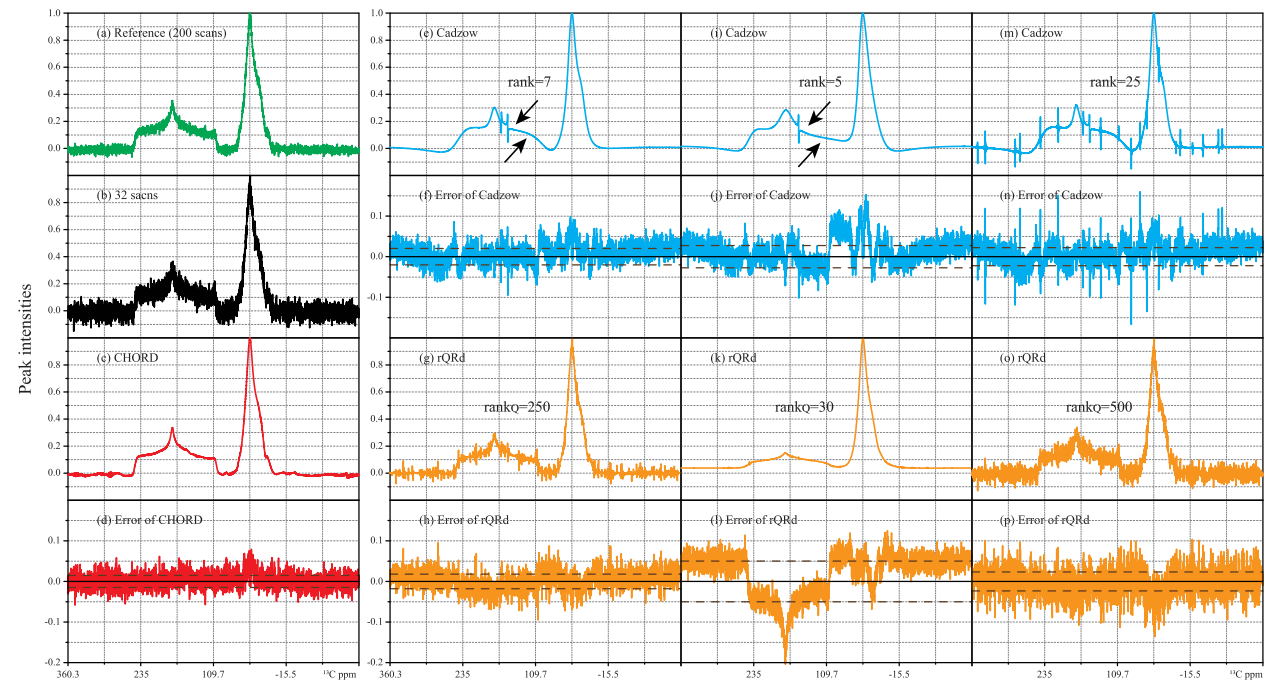


Fig. 18. Denoising of a ¹³C solid-state NMR spectra. (a) and (b) Reference spectrum (200 scans) and the observation (32 scans), respectively. (c) and (d) Denoised spectra and the error of CHORD with the suggested parameter. (e) and (f), (i) and (j), and (m) and (n) Denoised spectra and their errors of Cadzow with three different estimated ranks (optimal in terms of NRMSE, small, and large). (g) and (h), (k) and (l), and (o) and (p) Denoised results of rQRd with three different estimated ranks (optimal in terms of NRMSE, small, and large). The brown long dash lines denote the MAEs of the denoised spectra.

The experimental ¹³C solid-state NMR data is a decoupled static chemical shift anisotropy (CSA) spectrum with the sample of glycine and was acquired on a Bruker 600 MHz spectrometer (14.1 T) equipped with an AVANCE-III console. A commercial Bruker HX double-resonance magic angle spinning (MAS) probe with a 4-mm outer diameter rotor was used in the static for the experiments.

Compared with the reference spectrum (average of 200 scans), CHORD with the automatic parameter effectively removes noise and preserves the details of the spectrum [red lines in Fig. 18(c) and (d)], saving more than 80% of acquisition time. For Cadzow, its optimal denoised result (in terms of NRMSE) over-smooths the spectrum and generates some fake peaks [black arrows in Fig. 18(e)]. Reducing the estimate of the rank suppresses the fake peak, but causes a more serious loss of signal details. A large rank keeps more details but leads to more fake peaks. For rQRd, its optimal result remains too much residue, a smaller estimate of rank results in a smoother spectrum with the loss of signal details.

VI. CONCLUSIONS

Based on CHORD, a denoising method based on low-rank Hankel property of complex exponential signals, we attempt to figure out the bound of the regularization parameter, determine the empirical optimal constant, and estimate the standard derivation of the noise so that the users are able to apply CHORD with an auto-setting parameter. Experiments on synthetic complex exponential and realistic NMR spectroscopy data demonstrate that CHORD with the auto-setting parameter achieves more robust and accurate results compared with Cadzow and rQRd methods.

In this article, we did not discuss the effect of \mathbf{x}_0 at great length and had not provided a theoretical estimate of $\mathbb{E}\|\tilde{\mathbf{X}}\|_2$. For the future work, it is worthwhile to explore an accurate estimate of $\mathbb{E}\|\tilde{\mathbf{X}}\|_2$. Moreover, we are also interested in exploring the probability distribution of the spectral norm and extending the 1-D model in (2) to higher-dimensional signals since their acquisition costs relatively more time in applications. In addition, nonexponential signals, such as Gaussian signals, are very common in applications [36]. Denoising Gaussian signals would be very different. How to denoise this type of signals is important and worth to explore it in the future.

ACKNOWLEDGMENTS

The authors would like to thank Hengfa Lu for polishing writing and Zhangren Tu for preparing part of code for comparison. They would also like to thank You-Wei Wen, Haolin Zhan, and Xinlin Zhang for helpful discussions. In addition, the authors are grateful to editors and reviewers for valuable suggestions.

REFERENCES

- [1] A. Wegemann, C. Staat, J. Rapp, A. Heidsieck, A. Haase, and B. Gleich, "A portable NMR spectrometer with a probe head combining RF and DC capabilities to generate pulsed-field gradients," *IEEE Trans. Instrum. Meas.*, vol. 69, no. 10, pp. 8628–8636, Oct. 2020.
- [2] K. Inomata et al., "High-resolution multi-dimensional NMR spectroscopy of proteins in human cells," *Nature*, vol. 458, no. 7234, pp. 106–109, Mar. 2009.
- [3] O. Beckonert et al., "High-resolution magic-angle-spinning NMR spectroscopy for metabolic profiling of intact tissues," Nature Protocols, vol. 5, no. 6, pp. 1019–1032, Jun. 2010.
- [4] M. C. Preul et al., "Accurate, noninvasive diagnosis of human brain tumors by using proton magnetic resonance spectroscopy," *Nature Med.*, vol. 2, no. 3, pp. 323–325, Mar. 1996.

- [5] P. P. Man, C. Bonhomme, and F. Babonneau, "Denoising NMR time-domain signal by singular-value decomposition accelerated by graphics processing units," *Solid State Nucl. Magn. Reson.*, vols. 61–62, pp. 28–34, Jul. 2014.
- [6] F. Lam, Y. Li, and X. Peng, "Constrained magnetic resonance spectroscopic imaging by learning nonlinear low-dimensional models," *IEEE Trans. Med. Imag.*, vol. 39, no. 3, pp. 545–555, Mar. 2020.
- [7] L. Chiron, M. A. van Agthoven, B. Kieffer, C. Rolando, and M.-A. Delsuc, "Efficient denoising algorithms for large experimental datasets and their applications in Fourier transform ion cyclotron resonance mass spectrometry," *Proc. Nat. Acad. Sci. USA*, vol. 111, no. 4, pp. 1385–1390, Jan. 2014.
- [8] F. Lam and Z.-P. Liang, "A subspace approach to high-resolution spectroscopic imaging," *Magn. Reson. Med.*, vol. 71, no. 4, pp. 1349–1357, Apr. 2014.
- [9] J. Ying, J.-F. Cai, D. Guo, G. Tang, Z. Chen, and X. Qu, "Vander-monde factorization of Hankel matrix for complex exponential signal recovery—Application in fast NMR spectroscopy," *IEEE Trans. Signal Process.*, vol. 66, no. 21, pp. 5520–5533, Nov. 2018.
- [10] Y. Lu, S. Joshi, and J. M. Morris, "Noise reduction for NMR FID signals via Gabor expansion," *IEEE Trans. Biomed. Eng.*, vol. 44, no. 6, pp. 512–528, Jun. 1997.
- [11] J. A. Cadzow, "Signal enhancement composite property mapping algorithm," *IEEE Trans. Acoust., Speech, Signal Process.*, vol. 36, no. 1, pp. 49–62, Jan. 1988.
- [12] Y. Y. Lin and L. P. Hwang, "NMR signal enhancement based on matrix property mappings," J. Magn. Reson., Ser. A, vol. 103, no. 1, pp. 109–114, Jun. 1993.
- [13] J. Gillard, "Cadzow's basic algorithm, alternating projections and singular spectrum analysis," *Statist. Interface*, vol. 3, no. 3, pp. 335–343, 2010.
- [14] X. Qu, M. Mayzel, J.-F. Cai, Z. Chen, and V. Orekhov, "Accelerated NMR spectroscopy with low-rank reconstruction," *Angew. Chem. Int.*, vol. 54, no. 3, pp. 852–854, Jan. 2015.
- [15] Y. Huang et al., "A pure shift-based NMR method for transverse relaxation measurements on complex samples," *IEEE Trans. Instrum. Meas.*, vol. 69, no. 1, pp. 201–211, Jan. 2020.
- [16] H. Li, Y. Yang, H. Zhan, X. Lin, and Z. Chen, "Periodic artifact suppression for pure shift NMR spectroscopy," *IEEE Trans. Instrum. Meas.*, vol. 70, 2021, Art. no. 4000609.
- [17] D. Chen, Z. Wang, D. Guo, V. Orekhov, and X. Qu, "Frontispiece: Review and prospect: Deep learning in nuclear magnetic resonance spectroscopy," *Chem. Eur. J.*, vol. 26, no. 46, p. 10, Aug. 2020.
- [18] T. Qiu, Z. Wang, H. Liu, D. Guo, and X. Qu, "Review and prospect: NMR spectroscopy denoising and reconstruction with low-rank Hankel matrices and tensors," *Magn. Reson. Chem.*, vol. 59, pp. 324–345, Mar. 2021.
- [19] X. Qu et al., "Accelerated nuclear magnetic resonance spectroscopy with deep learning," Angew. Chem. Int., vol. 59, pp. 10297–10300, Jun. 2020.
- [20] H. Lu et al., "Low rank enhanced matrix recovery of hybrid time and frequency data in fast magnetic resonance spectroscopy," *IEEE Trans. Biomed. Eng.*, vol. 65, no. 4, pp. 809–820, Apr. 2017.
- [21] J. Ying et al., "Hankel matrix nuclear norm regularized tensor completion for N-dimensional exponential signals," *IEEE Trans. Signal Process.*, vol. 65, no. 14, pp. 3702–3717, Jul. 2017.
- [22] H. M. Nguyen, X. Peng, M. N. Do, and Z.-P. Liang, "Denoising MR spectroscopic imaging data with low-rank approximations," *IEEE Trans. Biomed. Eng.*, vol. 60, no. 1, pp. 78–89, Jan. 2013.
- [23] A. Santos-Díaz and M. D. Noseworthy, "Comparison of compressed sensing reconstruction algorithms for 31P magnetic resonance spectroscopic imaging," *Magn. Reson. Imag.*, vol. 59, pp. 88–96, Jun. 2019.
- [24] P. Cao et al., "Accelerated high-bandwidth MR spectroscopic imaging using compressed sensing," Magn. Reson. Med., vol. 76, no. 2, pp. 369–379, Aug. 2016.
- [25] J. P. Haldar, "Low-rank modeling of local k-space neighborhoods (LORAKS) for constrained MRI," *IEEE Trans. Med. Imag.*, vol. 33, no. 3, pp. 668–681, Mar. 2014.
- [26] X. Zhang et al., "Image reconstruction with low-rankness and self-consistency of k-space data in parallel MRI," Med. Image Anal., vol. 63, Jul. 2020, Art. no. 101687.
- [27] Y. Huang et al., "Phase-constrained reconstruction of high-resolution multi-shot diffusion weighted image," J. Magn. Reson., vol. 312, Mar. 2020, Art. no. 106690.
- [28] J. C. Lindon and A. G. Ferrige, "Digitisation and data processing in Fourier transform NMR," *Prog. Nucl. Magn. Reson. Spectrosc.*, vol. 14, no. 1, pp. 27–66, Jan. 1980.

- [29] D. L. Donoho, "De-noising by soft-thresholding," *IEEE Trans. Inf. Theory*, vol. 41, no. 3, pp. 613–627, May 1995.
- [30] D. Barache, J.-P. Antoine, and J.-M. Dereppe, "The continuous wavelet transform, an analysis tool for NMR spectroscopy," *J. Magn. Reson.*, vol. 128, no. 1, pp. 1–11, Sep. 1997.
- [31] D. L. Donoho, I. M. Johnstone, A. S. Stern, and J. C. Hoch, "Does the maximum entropy method improve sensitivity?" *Proc. Nat. Acad. Sci. USA*, vol. 87, no. 13, pp. 5066–5068, Jul. 1990.
- [32] K. Takeda, "Solid-state covariance NMR spectroscopy," Annu. Rep. NMR Spectrosc., vol. 84, pp. 77–113, Jan. 2015.
- [33] C. Kaiser, J. J. Lopez, W. Bermel, and C. Glaubitz, "Dual transformation of homonuclear solid-state NMR spectra—An option to decrease measuring time," *Biochimica Biophysica Acta*, vol. 1768, no. 12, pp. 3107–3115, Dec. 2007.
- [34] E. R. Malinowski, "Determination of the number of factors and the experimental error in a data matrix," *Anal. Chem.*, vol. 49, pp. 612–617, May 1977.
- [35] E. R. Malinowski, "Abstract factor analysis of data with multiple sources of error and a modified Faber–Kowalski f-test," *J. Chemometrics*, vol. 13, no. 2, pp. 69–81, Mar. 1999.
- [36] G. Laurent, W. Woelffel, V. Barret-Vivin, E. Gouillart, and C. Bonhomme, "Denoising applied to spectroscopies—Part I: Concept and limits," *Appl. Spectrosc. Rev.*, vol. 54, no. 7, pp. 602–630, Aug. 2019.
- [37] Y. Chen and Y. Chi, "Robust spectral compressed sensing via structured matrix completion," *IEEE Trans. Inf. Theory*, vol. 60, no. 10, pp. 6576–6601, Oct. 2014.
- [38] J. C. Hoch and A. S. Stern, *NMR Data Processing*. New York, NY, USA: Wiley, 1996.
- [39] P. Koehl, "Linear prediction spectral analysis of NMR data," Prog. Nucl. Magn. Reson. Spectrosc., vol. 34, nos. 3–4, pp. 257–299, 2009
- [40] J.-F. Cai, E. J. Candes, and Z. Shen, "A singular value thresholding algorithm for matrix completion," SIAM J. Optim., vol. 20, no. 4, pp. 1956–1982, 2010.
- [41] S. Boyd, N. Parikh, E. Chu, B. Peleato, and J. Eckstein, "Distributed optimization and statistical learning via the alternating direction method of multipliers," *Found. Trends Mach. Learn.*, vol. 3, no. 1, pp. 1–122, Jan. 2011.
- [42] G. A. Watson, "Characterization of the subdifferential of some matrix norms," *Linear Algebra Appl.*, vol. 170, pp. 33–45, Jun. 1992.
- [43] D. P. Bertsekas, A. Nedic, and A. E. Ozdaglar, Convex Analysis and Optimization. Belmont, MA, USA: Athena Scientific, 2003.
- [44] E. J. Candès and Y. Plan, "Matrix completion with noise," Proc. IEEE, vol. 98, no. 6, pp. 925–936, Jun. 2010.
- [45] M. Meckes, "On the spectral norm of a random Toeplitz matrix," Electron. Commun. Probab., vol. 12, pp. 315–325, Jan. 2007.
- [46] V. V. Nekrutkin, "Remark on the norm of random Hankel matrices," Vestnik St. Petersburg Univ., Math., vol. 46, no. 4, pp. 189–192, Oct. 2013.
- [47] J. A. Tropp, "An introduction to matrix concentration inequalities," Found. Trends Mach. Learn., vol. 8, pp. 1–230, May 2015.
- [48] W. Liao, "MUSIC for multidimensional spectral estimation: Stability and super-resolution," *IEEE Trans. Signal Process.*, vol. 63, no. 23, pp. 6395–6406, Dec. 2015.
- [49] T. Chai and R. R. Draxler, "Root mean square error (RMSE) or mean absolute error (MAE)?—arguments against avoiding RMSE in the literature," *Geosci. Model Develop.*, vol. 7, no. 3, pp. 1247–1250, Jun. 2014.
- [50] C. J. Willmott and K. Matsuura, "Advantages of the mean absolute error (MAE) over the root mean square error (RMSE) in assessing average model performance," *Climate Res.*, vol. 30, no. 1, pp. 79–82, Dec. 2005.
- [51] F. J. Massey Jr., "The Kolmogorov-Smirnov test for goodness of fit," J. Amer. Statist. Assoc., vol. 46, no. 253, pp. 68–78, 1951.
- [52] K. Kazimierczuk and V. Y. Orekhov, "Accelerated NMR spectroscopy by using compressed sensing," *Angew. Chem. Int.*, vol. 50, no. 24, pp. 5556–5559, Jun. 2011.
- [53] H. W. Engl, "Discrepancy principles for Tikhonov regularization of ill-posed problems leading to optimal convergence rates," *J. Optim. Theory Appl.*, vol. 52, no. 2, pp. 209–215, Feb. 1987.
- [54] Y.-W. Wen and R. H. Chan, "Parameter selection for total-variation-based image restoration using discrepancy principle," *IEEE Trans. Image Process.*, vol. 21, no. 4, pp. 1770–1781, Apr. 2012.
- [55] B. Li, L. Jin, C. Leng, C. Lu, and J. Zhang, "A smooth approximation algorithm of rank-regularized optimization problem and its applications," in *Proc. Int. Conf. Image Graph.*, 2015, pp. 470–479.



Tianyu Qiu received the B.S. degree in electronic science from Xiamen University, Xiamen, China, in 2016, where she is currently pursuing the Ph.D. degree with the Department of Electronic Science.

Her research interests include magnetic resonance spectroscopy reconstruction, signal processing, and physics of magnetic resonance.



Wenjing Liao received the B.S. degree in mathematics from Fudan University, Shanghai, China, in 2008, and the Ph.D. degree in applied mathematics from the University of California, Davis, CA, USA, in 2013.

Taking her position at Georgia Institute of Technology, Atlanta, GA, USA, she was with the Statistical and Applied Mathematical Sciences Institute, Durham, NC, USA, from 2013 to 2015, and Duke University, Durham, NC, from 2013 to 2016. She is currently an Assistant Professor with

the School of Mathematics, Georgia Institute of Technology. Her research interests include high-dimensional data analysis, machine learning, imaging, signal processing, inverse problems, and applied harmonic analysis and computational mathematics.



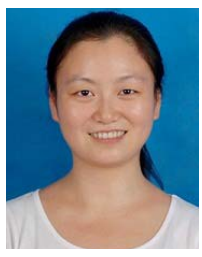
Yihui Huang received the B.S. and M.S. degrees from the Department of Biomedical Engineering, Southern Medical University, Guangzhou, China, in 2015 and 2018, respectively. He is currently pursuing the Ph.D. degree with the Department of Electronic Science, Xiamen University, Xiamen, China.

His research interests include deep learning and optimization to fast magnetic resonance imaging, magnetic resonance spectroscopy, and analysis.



Jinyu Wu received the B.S. degree from the School of Information Science and Engineering (ISE), Shandong University, Jinan, China, in 2020. She is currently pursuing the M.S. degree with the Department of Electronic Science, Xiamen University, Xiamen,

Her research interests include magnetic resonance spectroscopy, analysis, and prior knowledge.



Di Guo received the B.S. and Ph.D. degrees in communication engineering from Xiamen University, Xiamen, China, in 2005 and 2012, respectively.

From 2009 to 2011 and from 2018 to 2019, she was a Visiting Scientist with the Department of Electrical Engineering, University of Washington, Seattle, WA, USA. She is currently a Professor with the Department of Computer Science and Technology, Xiamen University of Technology, Xiamen. Her research was supported by the National Natural

Science Foundation of China and other grant agencies. Her research interests include signal and image processing, machine learning, artificial intelligence, and their applications in biomedical engineering, wireless sensor networks, and Internet of Things.

Dr. Guo was a recipient of the IBM Distinguished Student Award in 2012.



Dongbao Liu received the B.S. degree in electronic information engineering from Fujian Normal University, Fuzhou, China, in 2018, and the M.S. degree in electronic and communication engineering from Xiamen University, Xiamen, China, in 2021.

His research interests include magnetic resonance imaging, magnetic resonance spectroscopy, magnetic resonance spectroscopy imaging, and machine learning and data mining.



Xin Wang received the B.S. degree from Hubei University, Wuhan, China, in 2004, and the M.S. degree from Xiamen University, Xiamen, China, in 2007.

He is currently a Senior Engineer with the Research Center of Magnetic Resonance and Medical Imaging, Research Center for Molecular Imaging and Translational Medicine, and Department of Electronic Science, Xiamen University. His research interests include electrochemistry and nuclear magnetic resonance.



Jian-Feng Cai received the B.S. and M.S. degrees in computational mathematics from Fudan University, Shanghai, China, in 2000 and 2004, respectively, and the Ph.D. degree in mathematics from the Chinese University of Hong Kong, Hong Kong, in 2007.

Taking his position at The Hong Kong University of Science and Technology (HKUST), Hong Kong, he was with the National University of Singapore, Singapore, from 2007 to 2009, University of California, Los Angeles, Los Angeles, CA, USA, from 2009 to 2011, and The University of Iowa, Iowa

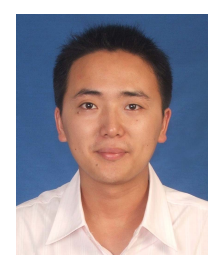
City, IA, USA, from 2011 to 2015. He was a Highly Cited Researcher in mathematics by Clarivate Analytics, London, U.K., from 2017 to 2018. He is currently a Professor with the Department of Mathematics, HKUST. His research interests include the design and analysis of efficient algorithms for real-world problems (e.g., data analysis, signal/image processing, machine learning), using tools from computational harmonic analysis, approximation theory, numerical linear algebra, optimization, and probability.



Bingwen Hu received the B.S. and M.S. degrees from the Department of Macromolecular Science, Fudan University, Shanghai, China, in 2003 and 2006, respectively, and the Ph.D. degree in nuclear magnetic resonance (NMR) from the Université de Lille, Lille, France, in 2009.

He is currently a Professor with the Department of Physics, East China Normal University, Shanghai, China. His research interests include solid-state NMR, lithium-ion batteries, solid-state electrochemistry, and electron paramagnetic reso-

nance (EPR) spectroscopy.



Xiaobo Qu (Member, IEEE) received the B.S. and Ph.D. degrees in communication engineering from Xiamen University, Xiamen, China, in 2006 and 2011, respectively.

From 2009 to 2011, he was a Visiting Scholar with the Department of Electrical and Computer Engineering, University of Illinois at Urbana-Champaign, Champaign, IL, USA. From 2012 to 2019, he was the short-term Visiting Professor with the University of Gothenburg, Gothenburg, Sweden, The Hong Kong University of Science and Technology,

Hong Kong, and the University of Washington, Seattle, WA, USA. Since 2012, he has been a Faculty Member with Xiamen University. He is currently a Professor and the Vice Director of the Department of Electronic Science, the Director of Biomedical Intelligent Cloud Research and Development Center, the Vice Director of Fujian Provincial Key Laboratory of Plasma and Magnetic Resonance, Xiamen University. His research interests include magnetic resonance imaging and spectroscopy, signal and image representations, computational imaging, machine learning, artificial intelligence and cloud computing.

Dr. Qu has been a member of ISMRM, IEEE EMBS, and SPS. He was a recipient of the Distinguished Young Scholar Award in Natural Science Foundation of Fujian Province of China (2018), the He Yici Chair Professor Award (2018) at Xiamen University, and the Excellent Young Scientists Fund Award from the National Natural Science Foundation of China (2021). He is an Associate Editor of the IEEE TRANSACTIONS ON COMPUTATIONAL IMAGING, and a Senior Editor of BMC Medical Imaging.